

PAPER

## Powering of an HTS dipole insert-magnet operated standalone in helium gas between 5 and 85 K




To cite this article: J van Nugteren *et al* 2018 *Supercond. Sci. Technol.* **31** 065002

View the [article online](#) for updates and enhancements.

### Related content

- [Progresses and challenges in the development of high-field solenoidal magnets based on RE123 coated conductors](#)  
Carmine Senatore, Matteo Alessandrini, Andrea Lucarelli *et al.*
- [Roebel cables from REBCO coated conductors: a one-century-old concept for the superconductivity of the future](#)  
Wilfried Goldacker, Francesco Grilli, Enric Pardo *et al.*
- [Conceptual designs of conduction cooled MgB<sub>2</sub> magnets for 1.5 and 3.0 Tesla full body MRI systems](#)  
Tanvir Baig, Abdullah Al Amin, Robert J Deissler *et al.*

# Powering of an HTS dipole insert-magnet operated standalone in helium gas between 5 and 85 K

J van Nugteren<sup>1</sup> , G Kirby<sup>1</sup>, H Bajas<sup>1</sup>, M Bajko<sup>1</sup>, A Ballarino<sup>1</sup>, L Bottura<sup>1</sup>, A Chiuchiolo<sup>1</sup>, P-A Contat<sup>1</sup>, M Dhallé<sup>2</sup>, M Durante<sup>3</sup>, P Fazilleau<sup>3</sup>, A Fontalva<sup>1</sup>, P Gao<sup>2</sup>, W Goldacker<sup>4</sup>, H ten Kate<sup>1</sup>, A Kario<sup>4</sup>, V Lahtinen<sup>5</sup>, C Lorin<sup>3</sup>, A Markelov<sup>6</sup>, J Mazet<sup>1</sup>, A Molodyk<sup>6</sup> , J Murtomäki<sup>1</sup>, N Long<sup>7</sup>, J Perez<sup>1</sup>, C Petrone<sup>1</sup>, F Pincot<sup>1</sup>, G de Rijk<sup>1</sup>, L Rossi<sup>1</sup>, S Russenschuck<sup>1</sup>, J Ruuskanen<sup>5</sup>, K Schmitz<sup>1</sup>, A Stenvall<sup>5</sup> , A Usoskin<sup>8</sup>, G Willering<sup>1</sup> and Y Yang<sup>9</sup>

<sup>1</sup>CERN, CH-1211 Geneva 23, Geneva, Switzerland

<sup>2</sup>University of Twente, Drienerlolaan 5, 7522NB Enschede, Netherlands

<sup>3</sup>CEA Saclay, Gif-sur-Yvette F-91191, Cedex, France

<sup>4</sup>Karlsruhe Institute of Technology, D-76131 Karlsruhe, Germany

<sup>5</sup>Tampere University of Technology, Korkeakoulunkatu 10, FI-33720 Tampere, Finland

<sup>6</sup>SuperOx, 20/2 Nauchnyi proezd, 117246 Moscow, Russia

<sup>7</sup>Victoria University of Wellington, PO Box 600 Wellington 6140, New Zealand

<sup>8</sup>Bruker HTS, Ehrlichstraße 10, D-63450 Hanau, Germany

<sup>9</sup>University of Southampton, University Road, Southampton SO17 1BJ, United Kingdom

E-mail: [jeroen.van.nugteren@cern.ch](mailto:jeroen.van.nugteren@cern.ch)

Received 19 January 2018, revised 8 March 2018

Accepted for publication 21 March 2018

Published 25 April 2018



CrossMark

## Abstract

This paper describes the standalone magnet cold testing of the high temperature superconducting (HTS) magnet Feather-M2.1-2. This magnet was constructed within the European funded FP7-EUCARD2 collaboration to test a Roebel type HTS cable, and is one of the first high temperature superconducting dipole magnets in the world. The magnet was operated in forced flow helium gas with temperatures ranging between 5 and 85 K. During the tests a magnetic dipole field of 3.1 T was reached inside the aperture at a current of 6.5 kA and a temperature of 5.7 K. These values are in agreement with the self-field critical current of the used SuperOx cable assembled with Sunam tapes (low-performance batch), thereby confirming that no degradation occurred during winding, impregnation, assembly and cool-down of the magnet. The magnet was quenched many tens of times by ramping over the critical current and no degradation nor training was evident. During the tests the voltage over the coil was monitored in the microvolt range. An inductive cancellation wire was used to remove the inductive component, thereby significantly reducing noise levels. Close to the quench current, drift was detected both in temperature and voltage over the coil. This drifting happens in a time scale of minutes and is a clear indication that the magnet has reached its limit. All quenches happened approximately at the same average electric field and thus none of the quenches occurred unexpectedly.

Keywords: superconducting magnets, superconducting accelerator magnets, high temperature superconductors, cold testing

(Some figures may appear in colour only in the online journal)

## 1. Introduction

Feather-M2 is an high temperature superconducting (HTS) accelerator dipole insert-magnet designed and constructed in the framework of EUCARD2 WP10.3 [1, 2], which serves as a test for an HTS conductor being part of a magnet. The magnet was designed to generate the required 5 T central magnetic field when operated when standalone, while maximizing the magnetic field contribution when operated inside a background field, for example supplied by the 13–15 T Fresca2 magnet [3–5]. To this purpose a novel layout type named aligned block is used [6, 7]. In this layout the HTS superconducting tapes are aligned with the magnetic field lines when the magnet is operated as insert inside a background magnetic field. This results in the engineering current densities being two to five times higher, compared to the unaligned case [8], but it should also reduce screening current effects, thereby improving magnetic field quality.

At present (summer 2017) the first two magnet poles named Feather-M2.1 and Feather-M2.2 have been wound, impregnated and assembled with a Roebel cable [9–13], cabled by SuperOx [14] using ReBCO coated conductor tape from Sunam [15], following the punch-and-coat route. This cable has a much lower (factor of three [16]) engineering current density than the final cable of the EuCARD2 program, whose tape was manufactured by Bruker HTS [17] and was assembled into Roebel cable by KIT [18]. This last cable was not available at the time of winding and will be tested in a magnet called Feather-M2.3–4 as a next step. Due to the low performance of the SuperOx/Sunam cable, the initial set of poles should be considered as practice coils in order to eliminate potential issues before using the more costly high performance cable. Winding of this cable onto the Feather-M2.3 and Feather-M2.4 poles is now foreseen in early 2018.

After assembly of the two poles, the Feather-M2.1–2 magnet was tested when standalone inside an iron yoke. Similar to the sub-scale prototype racetrack coil Feather-M0.4, tested last year at CERN [19], the magnet is operated inside forced flow helium gas with variable temperature. Despite the low performance of the cable, the cold powering tests offer valuable insight into the future use of HTS inside accelerator magnets, like FCC [20, 21]. This paper briefly presents the assembly of the Feather-M2.1–2 (SuperOx, Sunam) magnet, the results from the first cold powering test and the insights gained. For convenience, the specifications of the Feather-M2.1–2 magnet and SuperOx/Sunam cable are summarized in tables 1 and 2, respectively. The definition of the used parameters is provided in the respective figures 1 and 2. After the initial series of tests presented in this paper, a set of Hall probes and pick-up coils were installed in the magnet's aperture in order to perform magnetic measurements. The results of these additional tests, showing dynamic field effects, are published separately in [22].

## 2. Winding, impregnation and assembly

One of the important findings of EUCARD2 is that the classical fiber-glass epoxy insulation and impregnation

**Table 1.** Geometric specifications of the Feather-M2.1–2 magnet. The used parameters are clarified in figure 1. © 2015 IEEE. Reprinted, with permission, from [7], and adapted from [8].

Symbol	Value	Description
$\phi_{in}$	40.0 mm	Aperture diameter
$\phi_{out}$	99.0 mm	Outer diameter
$d_{ap}$	2.0 mm	Extra aperture spacing
$R_{yoke1}$	51.0 mm	Yoke inner radius
$R_{yoke2}$	111.0 mm	Yoke outer radius
$L_{yoke}$	800.0 mm	Yoke length
$n_{turn1}$	8	Central deck number of turns
$n_{turn2}$	4	Wing deck number of turns
$L_0$	100.0 mm	Straight section length
$L_w$	44.0 mm	Straight section width
$L_{co}$	720 mm	Total coil length
$y_{cen1}$	3.8 mm	Central deck y-position
$y_{cen2}$	17.3 mm	Wing deck y-position
$h_{end1}$	21.3 mm	Central deck flaring height
$h_{end2}$	21.3 mm	Wing deck flaring height
$a_{end}$	4.0°	Flaring angle at coil end
$a_{rot1}$	0.5°	Central shear angle
$a_{rot2}$	8.0°	Wing shear angle
$p_{twist}$	0.6	Shear angle factor
$R_{easy}$	16.0 mm	Easy-way bend radius
$R_{mid}$	400 mm	Mid-coil bend radius
$R_{hard}$	2000 mm	Hard-way bend radius
$l_{cen}$	12.2 m	Central deck cable length
$l_{wing}$	3.6 m	Wing deck cable length
$l_{lead}$	1.35 m	Length of each current lead
$l_{pole}$	18.5 m	Cable length in each pole
$l_{total}$	37 m	Total cable length in magnet
$L_{self}$	166 $\mu$ H	Magnet self-inductance
$E_{stored}$	2.9 kJ	Stored energy at 6 kA/3 T

**Table 2.** Geometric specifications of the used Roebel cable used in Feather-M2.1–2, assembled by SuperOx from Sunam tape. The used parameters are clarified in figure 2. © 2015 IEEE. Reprinted, with permission, from [7], and adapted from [8].

Symbol	Value	Description
$N_s$	15	Number of tapes
$d_s$	0.15 mm	Tape thickness
$d_c$	1.2 mm	Cable total thickness
$d_i$	0.1 mm	Insulation thickness
$W_r$	5.00 mm	Tape width
$W_t$	12.0 mm	Cable width
$W_x$	6.00 mm	Cross over width
$W_c$	2.0 mm	Channel width
$\Phi$	30°	Cross over angle
$L_{tp}$	300 mm	Transposition pitch
$r_i$	6.0 mm	Inner radius
$r_o$	0.0 mm	Outer radius

scheme can also be applied to HTS. To avoid high stresses due to the Lorentz forces on the complex cable geometry [24] it is necessary to fill all voids with epoxy resin. The resin spreads out the stresses and avoids scissoring and peel-off effects of the tapes along the edges at the cross-over locations.

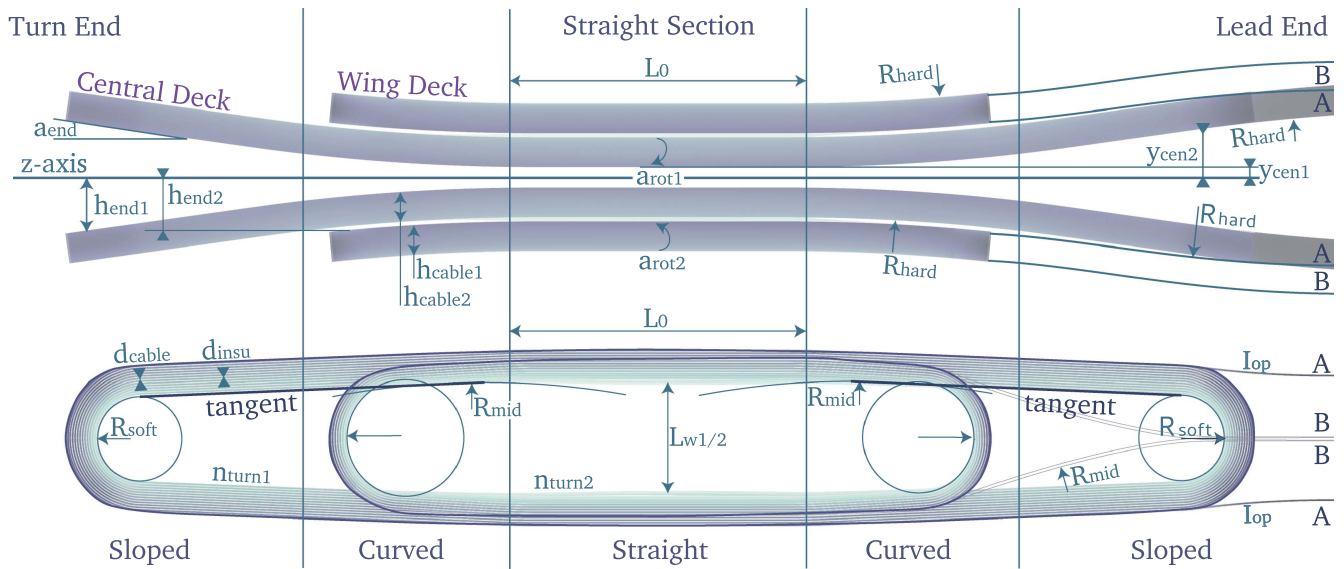


**Figure 1.** Side and top views on the geometry of the Feather-M2 coil and the definition of its geometric parameters. Respective values of the magnet tested are presented in table 1. Note that the illustration is not to scale. © 2015 IEEE. Reprinted, with permission, from [7], and adapted from [8].

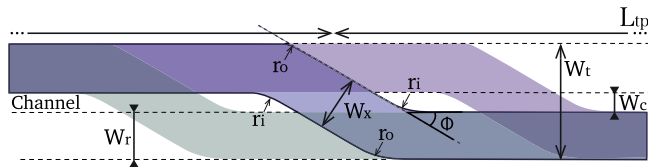


**Figure 2.** Definition of parameters for the geometry of a Roebel cable [23]. Respective values can be found in table 2. © 2015 IEEE. Reprinted, with permission, from [7], and adapted from [8].

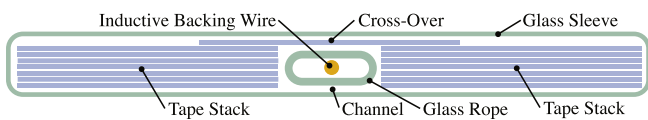


**Figure 3.** Illustration showing the cross-section of a Roebel cable, its nomenclature and the used insulation scheme.

To avoid delamination [25] of the tapes, it is important that the thermal contraction of the epoxy matches that of the tapes [26]. Therefore it was decided to use clear epoxy resin (CTD101K [27]) in combination with glass fibers (see figure 3). These glass fibers comprise a rope inside the channel at the center of the cable and a sleeve on the outside, which is also part of the turn-to-turn insulation. The resulting glass-fiber epoxy has about the same thermal contraction as copper and stainless steel. The resin was cured using the standard cycle of 5 h at 110 °C then 16 h at 125 °C. Using this scheme it was experimentally determined, by the University of Twente, that the coil pack can resist a transverse pressure exceeding 400 MPa [28, 29]. To avoid the impregnated coil pack being under tension, another suspected cause for delamination, it was decided to mold-release the central former. During the winding and impregnation the coil pack is put under a slight compression of 2–5 MPa in order to achieve good electrical contact between all the tapes. This is necessary

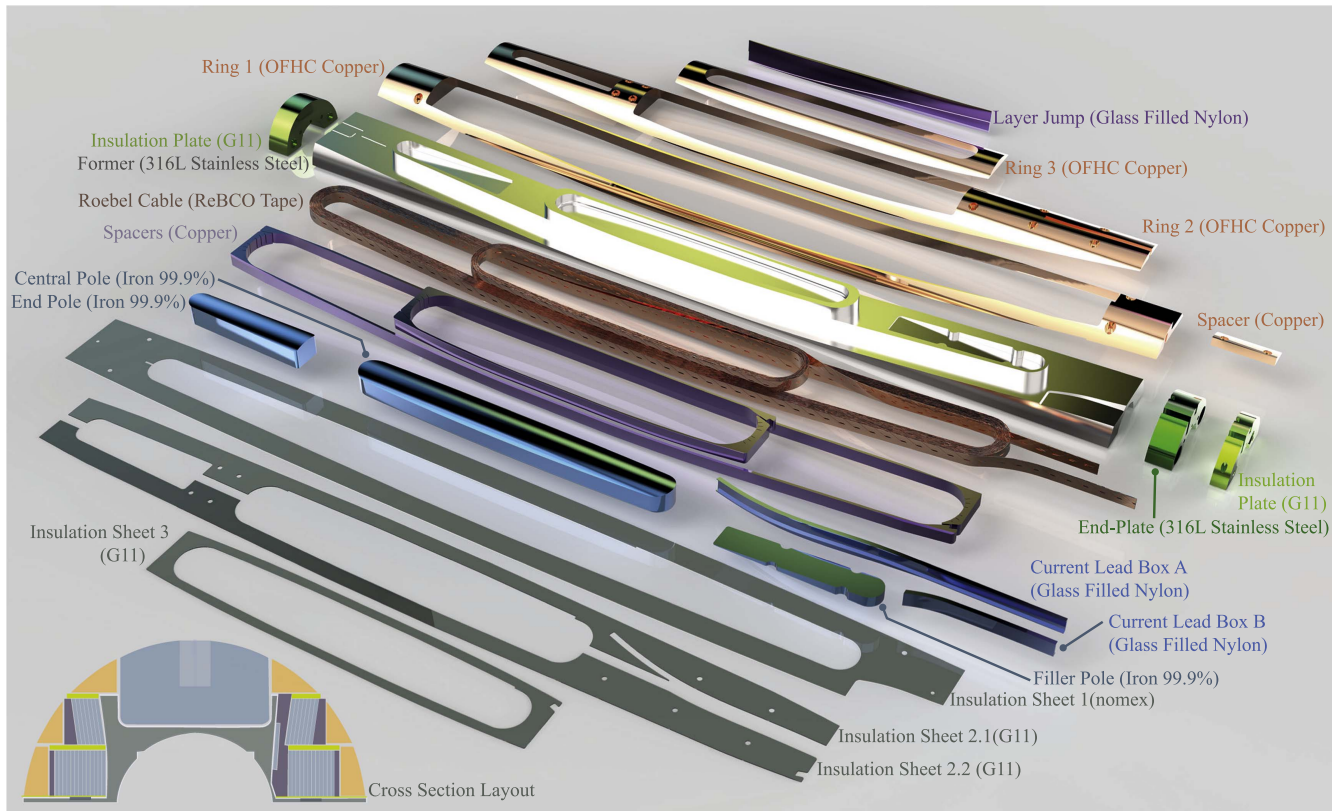
to improve the thermal stability of the coil and to allow current sharing between the tapes in case of small defects.

Figure 4 shows a rendering of the parts making up one magnet pole of the Feather-M2 magnet. The Roebel cable is wound onto a central former, as shown in figure 5. The cable is surrounded by a set of spacers, allowing the OFHC copper inductively coupled energy dissipation (ICED) rings [30–33] to be inserted from the top. A set of G11 sheets electrically insulate the decks from one another and from ground. Iron pole pieces are inserted to increase the magnetic field by another 0.4 T. The forces onto the end of the coil are intercepted by a set of stainless steel end-plates. Each pole of the magnet is wound on top of the impregnation mold, which when closed is by itself vacuum tight. This allows for impregnation without using a vacuum chamber. The impregnated coils, shown in figure 6, are assembled together inside an aluminum cylinder, which is responsible for containing the radial forces. The iron yoke was assembled around the magnet after which the current lead connections are made.

The resistances between coil, ground and instrumentation are in all cases in the range of 100 GΩ indicating that the used impregnation and insulation system is adequate. In addition a fast discharge test was performed, up to 2 kV, to check for turn-to-turn shorts. It was observed that the voltage recordings were similar between Feather-M2.1 and Feather-M2.2 for all amplitudes and thus no shorts were revealed.

### 3. Instrumentation and noise levels

Because quench detection and protection was a major concern, Feather-M2.1-2 features some instrumentation that is not very common for accelerator magnets. A simplified wiring diagram providing an overview of the instrumentation on the coils is shown in figure 7. Visible are the two main current leads A and B, part of the test facility, with the two coils,



**Figure 4.** Rendering showing an exploded view of all the parts making up one of the Feather-M2 magnet poles. Visible from top to bottom are the copper rings, the spacers, the coil-windings and joint area, the former, the iron poles and the G11 insulation sheets.



**Figure 5.** Photograph showing an overview of Feather-M2.1 during coil winding. Visible are the individual turns, the copper spacer and ring, the former and the winding and impregnation tooling.

Feather-M2.1 and Feather-M2.2 connected via an interlayer splice. Each of the leads, exiting the coils, has two voltage taps (for redundancy), forming a twisted pair with the wire of the opposing lead. The voltage taps are soldered to an arbitrary tape in the cable, which is not necessarily the same one on either side of the coil. Each lead is also equipped with a set of pick-up coils to measure fast changes of the current distribution between the tapes inside the cable. A temperature sensor is mounted inside the copper ring both on the lead-end and turn-end of each coil. These temperature sensors are used to determine the operating temperature of the magnet.

Additional temperature sensors are present on the main current leads and outside of the yoke. Inside the aperture a set of three Hall probes is present, each of which is backed by a pick-up coil to ensure proper calibration, as the used Hall probes are not stable during the variable temperature operation.

In order to measure only the resistive component of the voltage over the coils and greatly reduce the noise-to-signal ratio of the voltage taps, an inductive backing wire [34] was inserted inside the central channel of the used Roebel cable (see figures 3 and 8). This enamel coated copper wire follows exactly the same path as the cable and thus the induced voltage over it is the same. This voltage is then subtracted from the measured voltage over coil. The noise level measured is about one-third of the noise level of the differential signal between the two poles of the magnet, not using the subtraction from the inductive wire. Also as intended it contains a near zero inductive component making data analysis and *EI*-curve (average electric field, generated by the resistive transition, against current, see section 6) fitting much easier, thereby providing a useful tool for analysis. The measured noise level in the voltage signal of each pole, at a sampling frequency of about 3 Hz, is approximately  $2 \mu\text{V}$ , equaling an electric field of  $0.1 \mu\text{V m}^{-1}$ .

In addition to the temperature sensors, also optical fibers with Bragg gratings [35, 36], a relatively new temperature monitoring technique, were used on the outside of the coil to map the temperature of important components, such as the joints and the top of the coil. The temperature as measured by the optical fibers was in good agreement with the classical



Figure 6. Feather-M2.1-2 poles before applying the polyimide insulation sheet and insertion into its aluminum support cylinder.

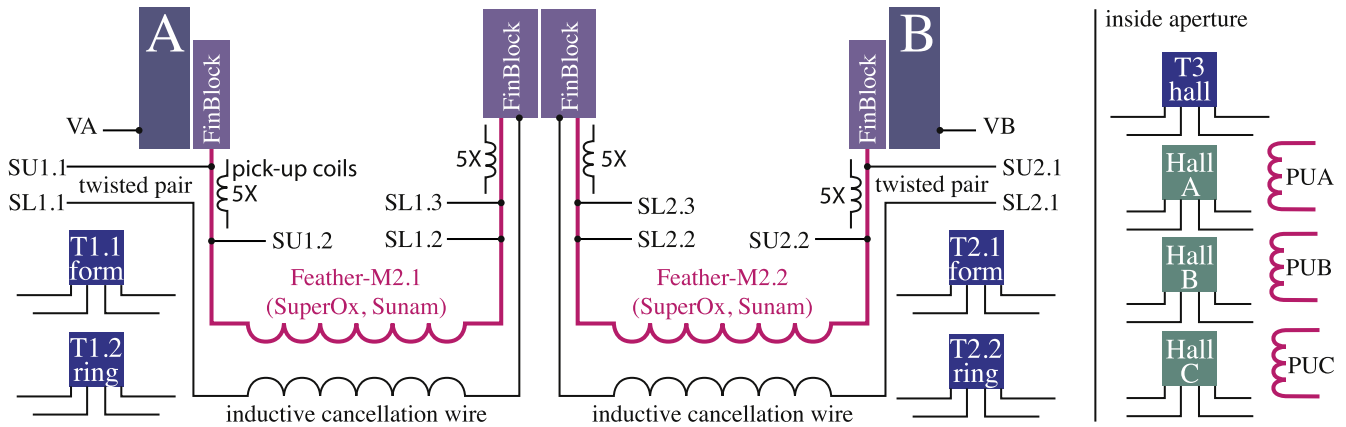


Figure 7. Simplified wiring diagram illustrating the instrumentation used in the Feather-M2.1-2 magnet.

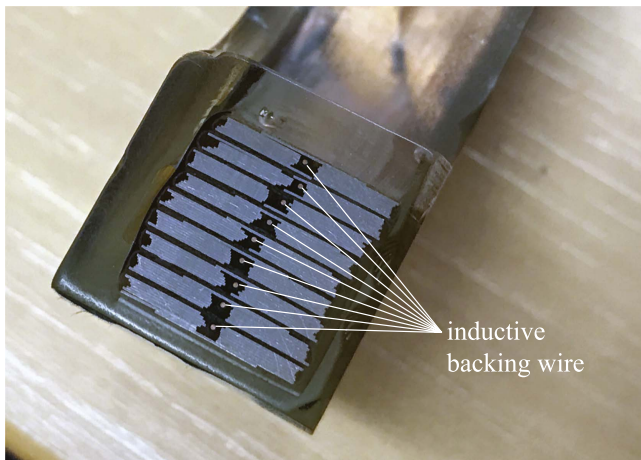


Figure 8. A cross-section of the impregnated coil pack with dummy Roebel cable. Visible is the inductive backing wire at the center of the cable.

temperature sensors, showing that the system is working correctly. For the next Feather-M2.3-4 coil it is planned to integrate these fibers inside the G11 insulation sheets to allow monitoring of local cable temperature rises during drift (see section 7).

#### 4. Cool-down, critical temperature and triple-R

The residual resistivity ratio (RRR) of the copper stabilizer reflects the purity and hardness state of the copper and is important to determine stability, losses and quench behavior of the magnets. Because of this, it is as well an important

input parameter for numerical models, to study, for example, quenches in HTS coils. The RRR is defined as the resistivity of the copper at 273 K divided with its resistivity at 10 K. To determine the RRR, the coil is powered during cool-down to a very low current of 6 A. By measuring the voltage drop over the coil the resistance of the cable can be determined as function of temperature. The cool-down of the magnet was performed in the time scale of several hours (approximate rate  $50 \text{ K h}^{-1}$ ) during which the temperature difference within the coil was kept within 20 K at all times. Below the critical temperature of 93 K the voltage drops to zero indicating that the coil is now fully superconducting. The transition observed is much more gradual than for low temperature superconducting (LTS) coils likely due to the top of the magnet being at a different temperature than the bottom of the magnet. This gradient was more prominent due to the higher heat capacity at 93 K compared to around 10 K, the critical temperature for Nb-Ti conductors. Because the cable becomes superconducting it is not possible to determine the resistance of the matrix below the critical temperature. Therefore, in order to determine RRR, it is necessary to perform a fit. The voltage over the cable at 6 A is calculated as function of temperature, for different triple-R values, using the copper resistivity relation from CUDI [37], which is based on [38], and the composition of the cable: 15 tapes, 5.0 mm wide, consisting of  $100 \mu\text{m}$  of Hastelloy and  $40 \mu\text{m}$  of copper (also see table 2). The measured voltage at temperatures of 300 K and  $\sim 98 \text{ K}$  (well above the transition) is compared to the calculated curves in figure 9. The measured voltages best match a copper RRR of  $20 \pm 5$ , which is in agreement with the expected value for the HTS tape [16].

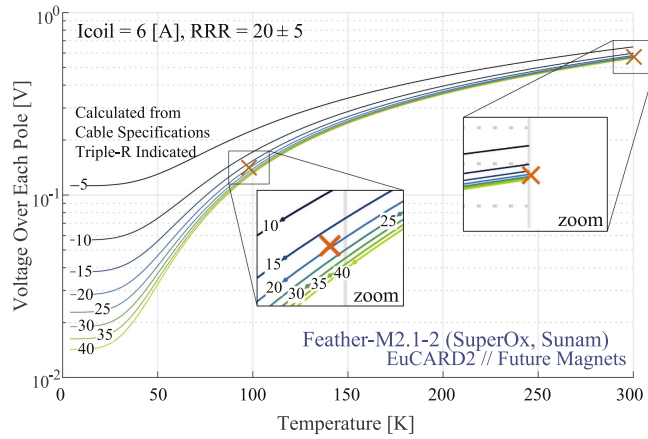


**Figure 9.** Determination of the RRR by fitting the calculated voltage against temperature curve against the voltage at room temperature and the voltage just before the superconducting transition, when running at 6 A. The calculation assumes similar conditions as in the coil: a 18.5 m long cable with 15 tapes, 5.5 mm wide, consisting of 100  $\mu\text{m}$  of Hastelloy and 40  $\mu\text{m}$  of copper. It can be seen that the RRR of the copper stabilizer is approximately  $20 \pm 5$ .

## 5. Training and degradation

During the testing the quench detection was set at a threshold voltage of 20 mV with an 8 ms delay time. After detection the current extraction was performed with a 50 m $\Omega$  dump resistor and 2.5 ms IGBT switch. These parameters were selected based on numerical simulations [8], which assume adiabatic conditions and should ensure safe operation of the magnet up to 12 kA, at which point the hot-spot temperature reaches an estimated 250 K. The peak temperature at the achieved operating current of 6 kA (see section 6) is approximately 160 K.

The magnet was quenched several tens of times at various temperatures and did not exhibit any training behavior. This is expected for HTS because it is many orders of magnitude more stable in terms of minimal quench energies. This means that suspected training mechanisms for LTS [39], for example, cracking of the resin or small conductor movements, cannot initiate a quench in HTS. Additionally, the quenches also did not lead to any degradation of the critical current, indicating that the used protection scheme is sufficient to protect the magnet.

## 6. Superconducting transition and critical current

The Feather-M2.1-2 magnet is tested in contrast to most LTS magnets in helium gas. This allows operation at variable temperature. At high temperatures, the critical current is very low and thus hot-spot temperatures rise slowly, leaving significant time for protection. At lower temperatures during a quench, the hot-spot temperature rises rapidly leaving little time for protection. By going down in temperature in steps, the quenches remain predictable, and thus risk to the magnet is minimized.

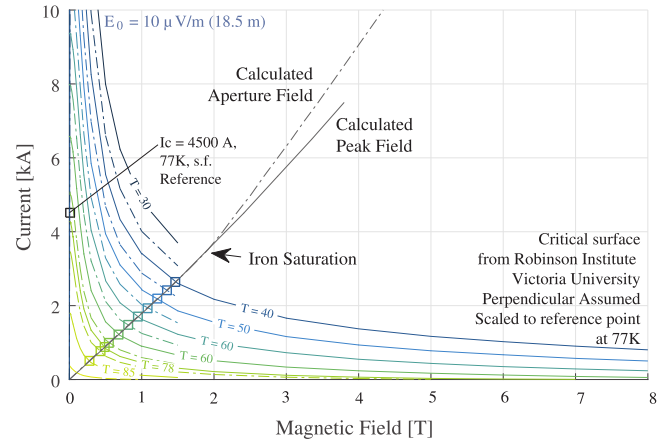


**Figure 10.** Prediction of the critical current using the critical surface of Sunam tape, data provided by the Robinson Institute, Victoria University, scaled to the self-field measurement at 77 K. The surface is assumed as perpendicular applied magnetic field. The intersections between the load-line of the magnet with the surface gives the critical current at each temperature.

The expected critical current of the Feather-M2.1-2 is calculated using the intersection between the load-line and the critical surface. However, because no explicit data was available on the used Sunam tape, a self-field critical current measurement was performed on a single 5.0 mm wide tape at 77 K. The critical current was determined at 300 A, making the estimated critical current of the cable approximately 4.5 kA (77 K, without self-field). This value was then used to scale the critical surface, based on measurement data a few years old [40], to match this value. The resulting critical surface, together with the calculated load-lines of the Feather-M2.1-2 magnet, is shown in figure 10. It can be seen that, at low magnetic fields, the critical current strongly depends on the applied magnetic field, and thus the self-field critical current is significantly higher than the critical current of the coil (even at half a Tesla). This can be explained by the choice of Sunam not to include artificial pinning centers (by doping) in their tapes.

The superconducting transition is commonly described by a power law which is given as  $E = E_0[I/I_c]^N$ , where  $I_c$  is the critical current,  $N$  is the so-called  $N$ -value,  $E$  is the electric field,  $I$  is the current in the conductor and  $E_0$  is the electric field criterion to define the critical current. Classically, in LTS applications, the electric field criterion is given as  $E_0 = 10 \mu\text{V m}^{-1}$ , which is the value also used in this paper. It must be noted, however, that in some other publications [41, 42], reporting HTS experiments, a criterion of  $100 \mu\text{V m}^{-1}$  is used. To determine the critical current the electric field in the coil is plotted against the current in a so-called  $EI$ -curve, which is defined here as the averaged electric field against the current in the coil, as opposed to an  $EJ$ -relation that describes the local behavior. This is important because it depends on the geometry of the coil: parts of the coil may have considerable less margin than other parts. As an example a measured  $EI$ -curve (using the non-inductive wire, see section 3) is shown, at an operating temperature of 7.9 K, in figure 11.

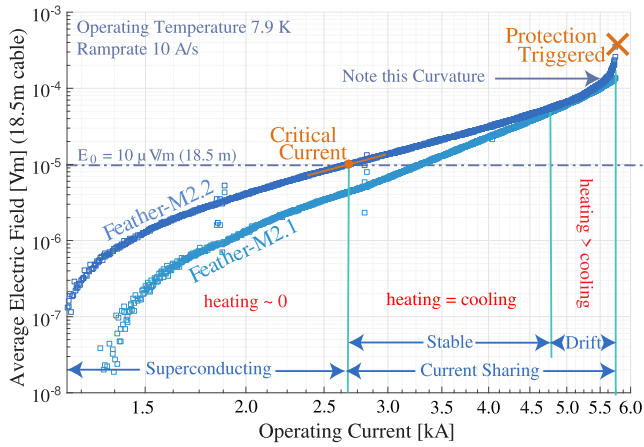


**Figure 11.** Measured average electric field versus current, showing the different heat-balance regimes, in the Feather-M2.1-2 at an operating temperature of 7.9 K in helium gas.

The critical current is then determined by fitting the power law to the data points near the transition. However, it can be seen that the magnet could be operated far beyond the critical current, as defined by  $E_0$ . The magnet ultimately quenches at a current which is around 160% of the critical current. Beyond the critical current there is a regime in which the superconductor transitions and thus an increasing amount of current is shared between the superconductor and the matrix, causing the magnet to be partially resistive. In this regime the electric heating is counteracted by the cooling power provided by the liquid or gas. When the heating and cooling are equal, the temperature is stable and the magnet can be operated indefinitely. When the heating exceeds the cooling, the temperature drifts away slowly over minutes until eventually a quench occurs. Similar results were reported in a cryogen-free (situation similar to gas)  $\text{MgB}_2$  coil in [43]. This type of behavior is much more apparent in HTS than in LTS due to the inherently soft transition (low  $N$ -value) and higher temperature margin. A temperature elevation, over that of the helium gas, allows a considerable amount of heat to be evacuated without triggering the typical runaway effect. This causes the region of stable current sharing to be quite extended.

It can be seen that towards higher current levels the  $EI$ -curve starts to deviate from the power law. This is likely due to the temperature continuously rising inside the coil. These assumptions are supported elevation of the coil temperature by a few kelvin with respect to the temperature of the helium gas, as measured by the regular temperature sensors located inside the copper rings (see section 8), as well as the optical fibers located outside at the lead end of the coil. This means that measuring and mapping the local temperature rise inside the coil, when inside or near the drift region, could yield very interesting results and should be considered for future HTS magnets.

To study the current sharing regime further, the fraction of current running in the superconducting and normal conducting part of the tapes can be estimated by the solution of a parallel path model [44, 45], in which the superconductor is

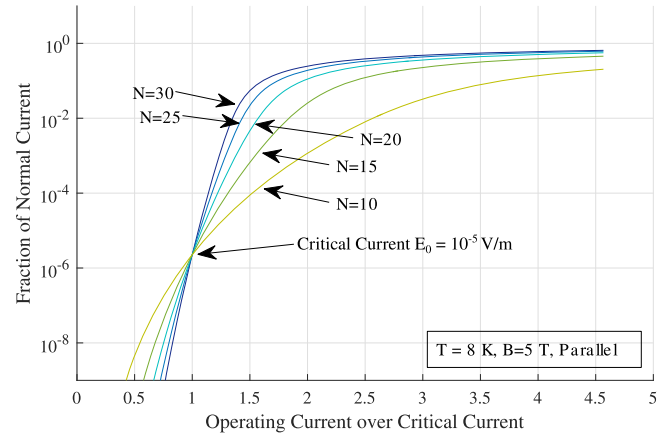


**Figure 12.** Calculated fraction of current flowing in the resistive part of the HTS tape as function of the operating current, which is normalized with the critical current, and  $N$ -value. A temperature of 8 K and 5 T parallel applied magnetic field are assumed.

modeled in parallel with the resistive materials. The resulting equation, describing the distribution of current between the paths, is given as

$$\frac{E_0}{\rho} \left[ \frac{I_{sc}}{I_c} \right]^N - I_{sc} = I_{tot}, \quad (1)$$

where  $E_0$  is the electric field criterion in  $\text{V m}^{-1}$ ,  $\rho$  the resistivity of the resistive part of the tape in  $\Omega \text{ m}^{-1}$ ,  $I_c$  the critical current of the conductor in A,  $N$  is the so-called  $N$ -value,  $I_{sc}$  the current flowing in the superconductor and  $I_{tot}$  the total current flowing in the conductor, both also in A. After solving numerically for  $I_{sc}$ , the normal conducting current can be calculated as  $I_{nc} = I_{tot} - I_{sc}$ . The resulting fraction of normal conducting current, as function of total current and  $N$ -value, is presented in figure 12. Note that the  $N$ -value of the individual tapes should be much higher, in the range of 20–30, than the  $N$ -value of the cable, which is around 6. It can be seen that considerable amount of current, about 1%, is flowing inside the matrix at about 1.3–1.6 (depending on  $N$ -value) times the critical current.

At each temperature the magnet is ramped at a rate of  $10 \text{ A s}^{-1}$  up to its quench current. Based on the resulting  $EI$ -curves the critical current and  $N$ -values are determined. The first are presented, together with the quench current and predicted critical current, as function of temperature in figure 13. Again the fully superconducting and current sharing regions are indicated. The predicted critical currents resulting from the load-line intersections with the scaled surface match well with the measured critical currents of the coil. This indicates that during coil construction no noticeable degradation has occurred. This is further confirmed by the very similar  $IV$ -characteristics between the two coils. In essence, the chances of having two coils with exactly the same degradation are very slim.

The resulting  $N$ -values are shown in figure 14. The  $N$ -value of the magnet is around 6. This is very low compared to LTS, where values of around 50 are expected, but even for HTS, which usually features  $N$ -values around 20–30 (for single tapes) [46]. This can be explained by the current



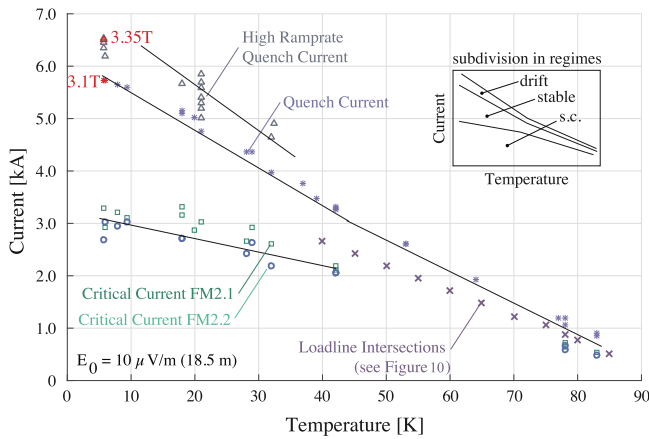


**Figure 13.** Measured quench and critical currents as function of temperature for the Feather-M2.1-2 (SuperOx, Sunam) high temperature superconducting magnet. Also shown are the load-line intersections from figure 10, which predict the critical current.

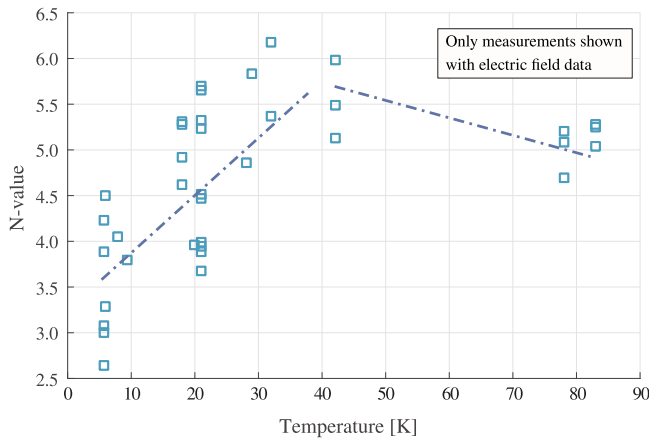


**Figure 14.** Measured  $N$ -values as function of temperature determined from the  $EI$ -curves measured on the Feather-M2.1-2 high temperature superconducting magnet.

distribution between all tapes in the cable in combination with different joint resistances for each tape [47]. It can be seen that the  $N$ -value of the coil has a slight dependence on the temperature. Towards the lower temperatures, the  $N$ -value likely goes down due to the reducing resistivity of the copper matrix, thereby favoring current sharing. At higher temperatures the  $N$ -value goes down because the distance with the critical temperature decreases. Further more accurate measurements on single tape and cable are required to confirm this observation and hypothesis.

The maximum current reached, at normal ramp-rate, was approximately 5.8 kA (also refer to figure 13) at which the magnetic field in the aperture is 2.9 T and the peak field is 3.1 T. For reference the calculated magnetic field in the aperture along the axis is shown as function of current in figure 15. At higher ramp-rates the quench current increases because less time is available for the coil pack to heat up in the current sharing regime. The increased coupling and hysteresis losses, causing LTS to quench at lower current at increased ramp-rates, have nearly no effect on HTS due to the much higher thermal margin. This causes the ramp-rate

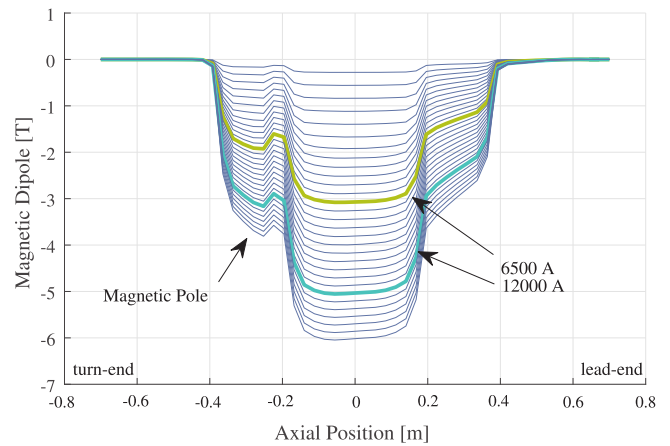


**Figure 15.** Calculated magnetic field along the length of the aperture for Feather-M2.1-2 as function of operating current. Highlighted is the achieved current of 6.5 kA and the design current, to be achieved with the Bruker cable, of 12 kA.

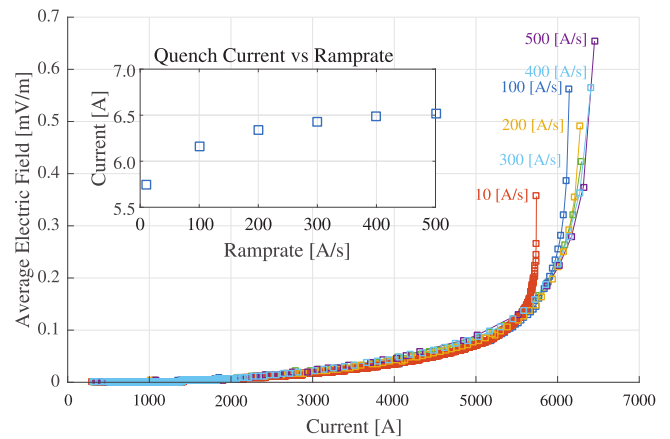


**Figure 16.** Measured dependence of the  $EI$ -curve on the ramp-rate at 5.7 K. It can be seen that at higher ramp-rate a higher quench current can be reached.

dependence of the quench current to be opposite between LTS and HTS. The quench current of Feather-M2.1-2 at an operating temperature of 5.7 K saturates at a value of about 6.5 kA (3.3 T peak field) with increased ramp-rate. The ramp-rate dependence is illustrated further in figure 16, which shows the different  $EI$ -curves. It can be seen that at high ramp-rate the curve can reach to a higher (quench) current. The curves start to deviate at around 5.5 kA, likely also the point at which the stable regime transitions into drift. Thereby the  $EI$ -curves can possibly be used to determine this point more easily.

## 7. Detecting the onset of a quench

One of the main goals for the magnet test was to determine whether it is possible to detect the onset of a quench. Here it is important to differentiate between a slow and global quench and a fast local quench [8]. The first can be detected by power dissipation in the coil, which is either visible directly by a voltage drop, or indirectly by a temperature rise. The second

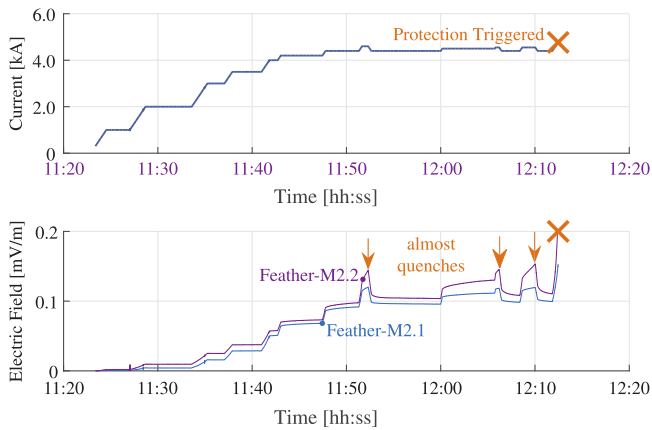


**Figure 17.** Measured average electric field and current as function of time demonstrating the typical behavior of an HTS magnet. It can be seen that the coil recovers three times (denoted with the arrows) by manually reducing the current just before a quench occurs. At the end of this dataset a real quench happens.

is local, for one or several tapes, and fast, with a time scale of 100 ms, and thus much harder to detect. This sort of quench causes a rapid sequence of current redistributions between the tapes and should therefore be visible by a signal on the pick-up coils. However, it is now believed that this type of quench may not occur at all due to the high power density required to initiate it.

During the measurement it was found that close to the quench current the voltages over the coil, as measured by the non-inductive wire, started to drift (also see figure 11). This drift was a clear indication of an imminent quench. The reaction time however is still on the time scale of several minutes and a small (100 A) reduction in operating current resulted in a recovery, as shown several times in the voltage recordings in figure 17. The exponential voltage increase before a quench could in principle be quantified by taking the first and second derivative of the voltage with respect to time. If both are positive a quench is imminent.

Additionally the average electric field at which the quenches occurred always exceeded  $200 \mu\text{V m}^{-1}$ , as shown in figure 18. In essence, all observed quenches were caused by ohmic heating due to over-current and thus none of the quenches occurred unexpectedly. Limiting the average electric field at a pre-set value in combination with the detection of temperature and/or voltage drifts could be a viable method in future HTS magnets to completely avoid quenching. This is an important observation and could be extremely useful when operating at very high current densities (well) exceeding  $1000 \text{ A mm}^{-2}$ , potentially enabling highly efficient (small cross-section) very high field accelerator magnets.

The pick-up coils did not see any signals prior to the fast discharge over the dump resistor. This could either be caused by the high noise floor of the used detection system (10 mV, 1 kHz) or by the absence of any current distribution during the quenches. The latter is likely the case since all quenches occurred at high average electric field. At this point all tapes inside the cable are partially resistive. The current distribution between the tapes is dominated by this resistance and thus all

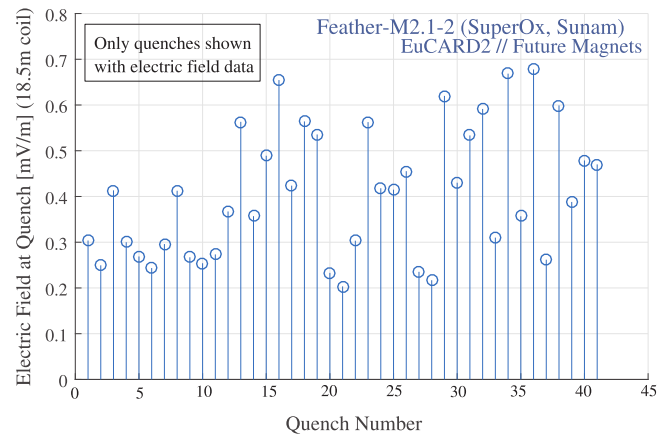


**Figure 18.** Measured average electric field just before the occurrence of a quench shown for a large selection of quenches in the Feather-M2.1-2 magnet. It can be seen that all quenches occurred above an average electric field of  $200 \mu\text{V m}^{-1}$ .

tapes are filled with current. An increase of the transport current or temperature more would quench all tapes simultaneously and thus no significant current redistribution would occur. A cable with a higher engineering current density may show much more redistribution of the current. Further experiments are expected to verify this.

## 8. Quench protection and copper ring

To reduce the decay time of the current, when extracting with a dump resistor a copper ICED ring was added around the coil pack (also see section 2). When the dump resistor is switched into the circuit, part of the current is transferred inductively into the ring, effectively extracting about 40% of the energy from the magnet, a concept often effectively applied to large solenoidal detector magnets. This could prove useful for future HTS magnets, where the extraction times limit the maximum current density and thus the efficiency of the magnet. Additional advantages are that the copper around the coil also provides extra cooling, through thermal conduction, and additional heat capacity, corresponding to reaction time, to the coil pack. Note that if an imminent quench can be reliably detected tens of seconds ahead of time, fast extraction and thus this type of system will not be necessary. Additionally, the copper rings could have a significant impact on the field quality due to induced currents during ramping and should be studied with care [22, 32].

Figure 19 presents the modeled and measured current decay of the Feather-M2.1-2 magnet. In the model the copper ring is included through a mutual inductance matrix assuming a coupling coefficient of 0.8. Additionally also the exponential LR-decay without copper ring is shown. It can be seen that the decay matches significantly better with the model including the copper ring. The temperature of the copper ring before and after a quench at 5.5 kA with an operating temperature of 8 K, is shown in figure 20. The temperature rise before the quench is caused by the heating of the coil pack during the drift. After the quench the temperature rises rapidly

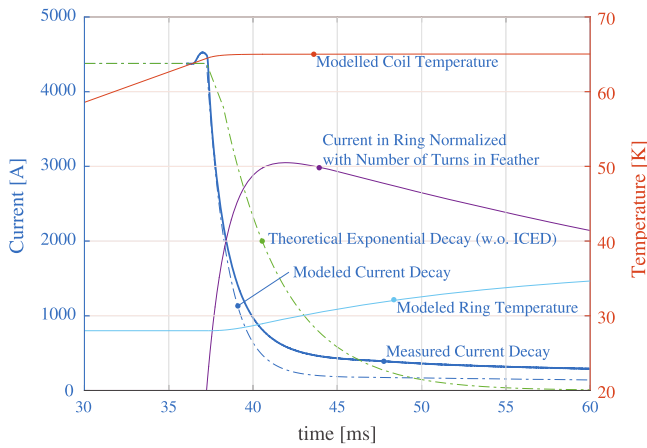


**Figure 19.** Comparison between the modeled and measured current decay after the switching of the dump resistor. It can be seen that the model including the copper ring is in good agreement with the measured data, while the theoretical exponential decay (not including the ring) fails to predict the behavior correctly.

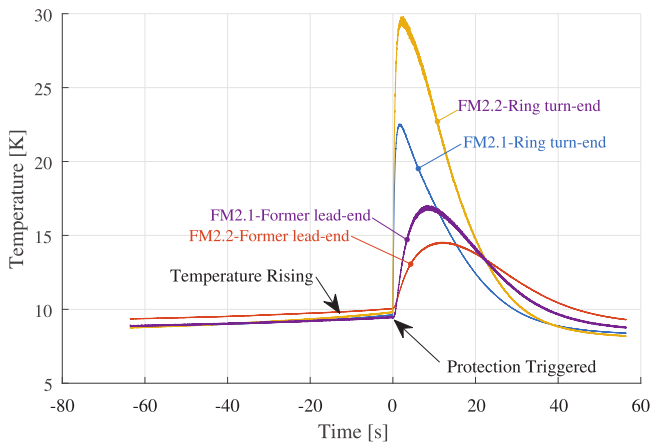


**Figure 20.** Measured temperature inside the copper rings and formers of Feather-M2.1-2 against time before and after the quench, which occurs at 0 s. It can be seen that before the quench, the temperature drifts away, after the quench a spike indicates that part of the energy has effectively been extracted by the copper rings.

up to 30 K due to the power dissipation in the ring. The temperature rise agrees well with numerical prediction. Based on the measured current decay, compared to numerical simulations, and the temperature rise of the ring, during extraction, it can be concluded that this concept is working as expected.

### 9. Joint resistances

A new joint system named Fin-Block [48] was used in the Feather-M2 magnet for the first time. During the testing the joints did not show any significant temperature rise and were not limiting the current, like they were in the Feather-M0.4 test [19]. Sub-cooling of the joints, as done in Feather-M0.4, was not necessary. The joint resistances are determined by linear fitting of the voltages against the current. The resulting

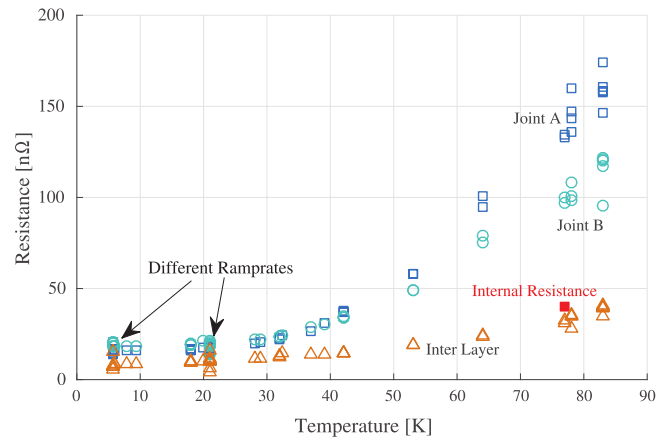


**Figure 21.** Joint resistances as function of temperature resulting from linear fitting of the measured voltages over the joints against the operating current of the magnet. See the electrical diagram in figure 7 for the location of the joints.

values are presented as function of temperature in figure 21. Joint resistances are all below 150 nΩ at 77 K and are below 19 nΩ at 10 K. This difference is caused by the resistivity of the copper, used for the various parts of the joint, which is strongly dependent on the temperature. Although the joints were no longer limiting the current, it must be noted that the Fin-Block configuration was much more difficult to handle during magnet assembly and in the test station than conventional joints due to its higher weight.

### 10. Conclusion

The full-scale coil Feather-M2.1-2 (SuperOx, Sunam) was successfully tested at variable temperature in helium gas up to a magnetic field of 3.1 T in the aperture and a magnetic peak field of 3.3 T on the conductor, which was reached at a temperature of 5.7 K and a current of 6.5 kA. These results demonstrate that with the performance of the next cables of EuCARD2 (tape processed by Bruker and cable assembled by KIT), which are presently being wound into the next coils Feather-M2.3-4, the EUCARD2 requirement of 5 T should easily be achieved.

The non-inductive backing wire has about one-third of the noise level than the differential signal between the two poles of the magnet. This type of measurement is useful for analysis of the behavior of the coil and should be considered for all magnets. A large, approximately factor 1.6, difference was found between the fitted critical current, at the traditional electric field criterion of  $10 \mu\text{V m}^{-1}$ , and the quench current. Beyond the critical current an increasing amount of current is shared with the resistive part of the conductor, causing the magnet to become partially resistive, resulting in heating. The current sharing can be subdivided further in a stable zone and a drift zone. In the stable zone the heat balance between heating and cooling result in a stable temperature, and thus the magnet can be operated indefinitely. In the drift zone the heating exceeds the cooling, causing the temperature in the coil to rise over a time scale of minutes, eventually leading to a quench.

The critical current of the coil is compared to experimental Sunam critical current data, appropriately scaled using a 77 K measurement. The critical currents resulting from the load-line intersections match well with the measured critical currents of the coil. This indicates that during coil construction no degradation has occurred in vital locations. In addition, both coils have very similar  $V-I$  characteristics, which further confirms that no degradation of the critical current occurred during construction.

The magnet was quenched several tens of times and did not exhibit any training behavior. This means that suspected training mechanisms for LTS, like cracking of the resin, do not initiate a quench in HTS. Also no degradation of the critical current was observed indicating that the protection scheme was sufficient. The onsets of the quenches were clearly visible by an exponential increase of the voltage many seconds in advance. In addition a temperature increase was observed both on classical temperature probes and on optical fibers. When the current is ramped down by a small amount (only 100 A) just before the quench, the magnet is able to recover.

## ORCID iDs

J van Nugteren  <https://orcid.org/0000-0001-8072-7725>

A Molodyk  <https://orcid.org/0000-0001-6313-6536>

A Stenvall  <https://orcid.org/0000-0001-7016-7648>

## References

- [1] Rossi L *et al* 2014 The EuCARD-2 Future Magnets project: the European collaboration for accelerator quality HTS magnets *IEEE Trans. Appl. Supercond.* **25** 4001007
- [2] Kirby G *et al* 2016 Status of the demonstrator magnets for the EuCARD-2 Future Magnets project *IEEE Trans. Appl. Supercond.* **26** 4003307
- [3] Ferracin P *et al* 2013 Development of the EuCARD Nb<sub>3</sub>Sn dipole magnet FRESCA2 *IEEE Trans. Appl. Supercond.* **23** 4002005
- [4] Rochepault E *et al* 2018 Mechanical analysis of the FRESCA2 dipole during preload, cool-down, and powering *IEEE Trans. Appl. Supercond.* **28** 4002905
- [5] Willering G *et al* 2018 Cold powering tests and protection studies of the FRESCA2 100 mm bore Nb<sub>3</sub>Sn block-coil magnet *IEEE Trans. Appl. Supercond.* **28** 4005105
- [6] Koski A and Wipf S L 1996 Computational design study for an accelerator dipole in the range of 15–20 T *IEEE Trans. Magn.* **32** 2159–62
- [7] van Nugteren J *et al* 2015 Study of a 5 T research dipole insert-magnet using an anisotropic ReBCO Roebel cable *IEEE Trans. Appl. Supercond.* **25** 4000705
- [8] van Nugteren J 2016 High temperature superconductor accelerator magnets *PhD Thesis* University of Twente
- [9] Roebel L 1915 Electrical conductor *US Patent* 1,144,252
- [10] Albrecht C, Masek P and Kummeth P 2004 Fully transposed high  $T_c$  composite superconductor, method for producing the same and its use *US Patent* USOO6725071B2
- [11] Long N J, Badcock R A, Bumby C and Jiang Z 2012 Production and characterisation of HTS Roebel cable *Superconductivity: Recent Developments and New Production Technologies* (Hauppauge, NY: Nova Publishers) ch 13
- [12] Goldacker W *et al* 2007 ROEBEL assembled coated conductors (RACC): preparation, properties and progress *IEEE Trans. Appl. Supercond.* **17** 3398–401
- [13] Fleiter J, Ballarino A, Goldacker W and Kario A 2014 Characterization of Roebel cables for potential use in high-field magnets *IEEE Trans. Appl. Supercond.* **25** 4802404
- [14] SuperOx 2018 *2G HTS Tape Performance and Specifications* (Moscow: SuperOx)
- [15] Lee H, Lee J-H, Chung W, Cheon K and Seung H M 2017 Recent highlights from SuNAM HTS Conductor & Magnet Accelerator Physics Meeting (Hong Kong)
- [16] Senatore C *et al* 2016 Field and temperature scaling of the critical current density in commercial REBCO coated conductors *Supercond. Sci. Technol.* **29** 014002
- [17] Bruker 2018 *HTS Tapes, YBCO Coated Conductors* (Hanau: Bruker)
- [18] Goldacker W, Grilli F, Pardo E, Kario A, Schlachter S I and Vojenčiak M 2014 Roebel cables from REBCO coated conductors: a one-century-old concept for the superconductivity of the future *Supercond. Sci. Technol.* **27** 093001
- [19] Kirby G *et al* 2017 First cold powering test of REBCO Roebel wound coil for the EuCARD2 Future Magnet development project *IEEE Trans. Appl. Supercond.* **27** 4003307
- [20] Barletta W *et al* 2014 Future hadron colliders: from physics perspectives to technology R&D *Nucl. Instrum. Methods Phys. Res. A* **764** 352–68
- [21] Schoerling D *et al* 2015 Strategy for superconducting magnet development for a future hadron-hadron circular collider at CERN *European Physical Society Conf. on High Energy Physics (Vienna, Austria, 22–29 July 2015)*
- [22] Petrone C *et al* 2018 Measurement and analysis of the dynamic effects in an HTS dipole magnet *IEEE Trans. Appl. Supercond.* (<https://doi.org/10.1109/TASC.2018.2801325>)
- [23] Lombardo V *et al* 2011 Fabrication, qualification and test of high  $J_c$  Roebel YBa<sub>2</sub>Cu<sub>3</sub>O<sub>7- $\delta$</sub>  coated conductor cable for HEP magnets *IEEE Trans. Appl. Supercond.* **21** 2331–4
- [24] Uglietti D, Wesche R and Bruzzone P 2013 Effect of transverse load on the critical current of a coated conductor Roebel cable *Supercond. Sci. Technol.* **26** 074002
- [25] Takematsu T *et al* 2010 Degradation of the performance of a YBCO-coated conductor double pancake coil due to epoxy impregnation *Physica C* **470** 674–7
- [26] Barth C *et al* 2013 Degradation free epoxy impregnation of REBCO coils and cables *Supercond. Sci. Technol.* **26** 055007
- [27] Composite Technology Development 2014 *CTD-101K Epoxy Resin System* (Lafayette, CO: Composite Technology Development)
- [28] Otten S 2014 Transverse pressure dependence of the critical current in epoxy impregnated ReBCO Roebel cables *Master's Thesis* University of Twente
- [29] Otten S, Dhallé M, Gao P, Wessel W, Kario A, Kling A and Goldacker W 2015 Enhancement of the transverse stress tolerance of REBCO Roebel cables by epoxy impregnation *Supercond. Sci. Technol.* **28** 065014
- [30] Gupta M *et al* 2014 High field HTS solenoid for a muon collider demonstrations, challenges, and strategies *IEEE Trans. Appl. Supercond.* **24** 4301705
- [31] Kirby G *et al* 2014 Accelerator quality HTS dipole magnet demonstrator designs for the EuCARD-2, 5 T, 40 mm clear aperture magnet *IEEE Trans. Appl. Supercond.* **25** 4000805
- [32] Murtomaki J, van Nugteren J, Kirby G, Stenvall A, Rossi L and de Rijk G 2016 Inductively coupled energy dissipater (ICED) for future high field accelerator magnets *Technical Report* EDMS 1607672 (CERN)

- [33] Ruuskanen J, Stenvall A, van Nugteren J and Lahtinen V 2018 Optimization of an  $E^3$ SPreSSO energy-extraction system for high-field superconducting magnets *IEEE Trans. Appl. Supercond.* **28** 4700805
- [34] Willering G *et al* 2014 Fast cycled magnet demonstrator program at CERN: instrumentation and measurement campaign *IEEE Trans. Appl. Supercond.* **24** 4004405
- [35] Hunte F, Song H and Schwartz J 2009 Fiber Bragg optical sensors for YBCO applications *Proc. 9th Int. Particle Accelerator Conf.* pp 3675–7
- [36] Chiuchiolo A *et al* 2014 Fiber Bragg grating cryosensors for superconducting accelerator magnets *IEEE Photonics J.* **6** 0600310
- [37] CERN 1992 CUDI: Users Manual
- [38] McAshan M S 1988 MIITS integrals for copper and for Nb-46.5 wt%Ti *Technical Report* SSC-N-468 (Fermilab, SSC Central Design Group)
- [39] Wilson M 1983 *Superconducting Magnets* (Oxford: Clarendon) ch 5
- [40] Wimbush S and Strickland N 2017 A public database of high-temperature superconductor critical current data *IEEE Trans. Appl. Supercond.* **27** 8000105
- [41] Hu D *et al* 2016 Modeling and comparison of in-field critical current density anisotropy in high-temperature superconducting (HTS) coated conductors *IEEE Trans. Appl. Supercond.* **26** 6600906
- [42] Grilli F *et al* 2014 Computation of losses in HTS under the action of varying magnetic fields and currents *IEEE Trans. Appl. Supercond.* **24** 78–110
- [43] Stenvall A *et al* 2007 A checklist for designers of cryogen-free  $MgB_2$  coils *Supercond. Sci. Technol.* **20** 386–91
- [44] Stekly Z J J and Zar J L 1965 Stable superconducting coils *IEEE Trans. Nucl. Sci.* **12** 367–72
- [45] Russenschuck S 2010 *Field Computation for Accelerator Magnets* (New York: Wiley)
- [46] Ghosh A K 2004  $V$ - $I$  transition and  $n$ -value of multi-filamentary LTS and HTS wires and cables *Physica C* **401** 15–21
- [47] Willering G *et al* 2015 Effect of variations in terminal contact resistances on the current distribution in high-temperature superconducting cables *Supercond. Sci. Technol.* **28** 035001
- [48] Murtomäki J *et al* 2018 10 kA joints for HTS Roebel cables *IEEE Trans. Appl. Supercond.* **28** 4801406